Short communications

Novel, large area scalable polycrystalline $Zn_{1-x}Co_xO$ films RF sputtered from a single mixed target for electrochemical water oxidation

Received 00th January 20xx,
Accepted 00th January 20xx

J. Pfrommer[a+], A. Steigert[b+], C. Goebel[a], I. Lauermann[b], W. Calvet[b], R. Klenk[b], S. Mikhailov[b], A. Azarpira[b], S. Selve[a], M. Lublow[b], Th. Schedel-Niedrig[b] , and M. Driess[a]

The compound semiconductor $Zn_{1-x}Co_xO$ (x= 0.42; ZnO:Co) has recently gained interest as a highly active electrocatalyst material for water oxidation (WOCs). We report on the significant structural and electronic transformations under anodic oxygen evolution reaction conditions of a novel, large area scalable sputtered ZnO:Co electrocatalyst. ZnO:Co sputtered films showed the transition of the polycrystalline ZnO:Co electrocatalyst material to a partially amorphous nanocomposite (ZnO:Co/$Co(OH)_2$/CoOOH). A high reactivity of the electrocatalyst material compensates effectively the low specific surface area of sputtered electrocatalyst thin films. The aim of this work is to examine the polycystral morphology of sputtered electrocatalyst thin film material, which can be also produced industrially on large areas and has a high WOC performance.

Water splitting is considered to be the key reaction in regard to storing solar energy as solar fuel.[1] There are many recent publications on hydrogen evolution reaction (HER) by solar water splitting using heterogeneous photocatalysts based on earth-rich transition metals with good performance.[2] The anodic oxygen evolution reaction (OER) is a kinetically unfavorable four electron process which contributes to a high overpotential above the thermodynamic limit (1.23 V vs. reversible hydrogen Electrode (RHE)) of the OER.[3] A great number of water oxidation catalysts (WOC) based on earth abundant early transition metals were described over the last years.[4] They were usually prepared in the form of nanoparticulate powders with a large specific surface area.[4,5] It is possible to fabricate small electrodes for lab scale electrochemical experiments with the use of binders (e.g. Nafion™)[4] or other methods (e.g. sintering, pressing, dip coating[6], screen printing[7]). These methods can have a profound influence on the catalyst (reaction with binder, change of grain boundaries, and reaction with solvents) and these electrodes cannot be considered of any applicability in larger scale setups. This is due to the often-complex preparation methods of the WOC particles and due to the error prone fabrication of the electrodes. There are several reports of electroplated WOCs, the coating of large arrays is challenging with this method and substrates must be compatible with the plating conditions (i.e. conductive, resistant to plating bath).[8] Methods for large scale coating with metal oxides such as chemical vapor deposition (CVD), plasma enhanced vapor deposition (PE-CVD) and sputter processes are well established for industrial scale thin film fabrication processes.[9] Examples for OER active thin films fabricated with these methods are scarce.[10] This is due to the low specific surface area of the resulting, densely packed two dimensional (2D) layers, which lack sufficient electrocatalytically active surface area.[11,12,13] In this work, we present a novel sputtered ZnO:Co electrocatalyst material that can circumvent this problem by undergoing significant structural and electronic transformations under anodic OER conditions, forming a partially amorphous nanocomposite as the active WOC *in operando*.

ZnO:Co compounds have been studied initially because they can be used as green pigment.[14] Most of the recent literature is concerned with the magnetic properties of the material (diluted magnetic semiconductor for spintronic).[15] Previous work on solvolytically prepared ZnO:Co nanoparticles showed them to be a suitable electrocatalyst for highly active OER catalyst composites. At anodic potentials, Zn was found to dissolve into the electrolyte and in a self-limiting process, a stable nanocomposite of crystalline ZnO:Co particles and amorphous $Co(OH)_2$/CoOOH was formed.[16,17]

It has already been shown that ZnO:Co ($Zn_{1-x}Co_xO$ x ≈ 0.2) thin films can be prepared by pulsed DC sputtering from a single target. Based on our positive experience with RF sputtering of Zn(O,S)[18] we have chosen this method as a possible alternative to the solvolytical preparation of highly Co substituted ZnO:Co materials in regard to reproducibility and purity of the resulting electrocatalyst films.[16] Direct growth of sputtered layers on conductive substrates also eliminates the error prone step of electrode fabrication from a suspension of catalyst particles.

[a] *Technische Universität Berlin, Straße des 17.Juni 115, 10623 Berlin, Germany*
[b] *Helmholtz-Zentrum Berlin GmbH, Hahn-Meitner-Platz 1, 14109 Berlin, Germany*
† *These authors contributed equally.*

Electronic Supplementary Information (ESI) available: SEM, TEM, SAED, EDX, GI_XRD, UV-VIS and … See DOI: 10.1039/x0xx00000x

To fabricate ZnO:Co thin films, a mixed target with a diameter of 75 mm and a nominal composition of Co/(Co+Zn) = 0.4 (atomic ratio) was procured from a commercial supplier. Films were sputtered in pure Ar using 13.56 MHz (RF) plasma excitation onto fluorine doped tin oxide (FTO; SnO_2:F) glass substrates, polycrystalline Si wafers and Mo sheets to show the substrate flexibility of this method. The base pressure in this UHV system was better than 5 x 10^{-9}mbar. The substrate was not moving during deposition. All depositions were performed at a constant power of 60 W resulting in a deposition rate of 40 nm min^{-1} and the deposition time was adjusted for a film thickness of 300 nm. To investigate the influence of the deposition parameters, the substrate temperature was changed between room temperature and 200°C and the Ar flow was varied in the range of 25 to 100 sccm (See SI Table S1). Regardless of the substrate, the deposited films were uniform 2D nanolayers without any porosity or additional structural features (see SEM Fig. S1)

The film composition was examined by powder x-ray diffraction (P-XRD, Fig S2) and UV-VIS spectroscopy (Fig S3). Both methods confirmed the formation of ZnO:Co on the substrates. The grazing-incidence (GI)-XRD (Fig. S4) showed the sputtered film to have a hexagonal wurtzite lattice ($P6_3mc$). In the UV-VIS, distinct absorption features (575 nm, 620 nm, 665 nm) were observed in the VIS region of the spectrum. This triple absorption band is indicative of Co^{2+} in T_d coordination.[19] Inductively coupled plasma optical emission spectroscopy (ICP-OES) and energy dispersive X-ray spectroscopy (EDX) revealed a Co content within the deposited films close to that of the ZnO/CoO sputter target (x_{Co}= 0.4).

To gain further insight into the sputtered ZnO:Co films, electron transparent samples were prepared from ZnO:Co films sputtered on polycrystalline silicon substrates (polycrystalline silicon allows better processing for electron transparent samples). Transmission electron microscopy (TEM) analysis of cross sections prepared from a nominally 300 nm ZnO:Co film shows an actual thickness of 250 nm and a columnar growth of crystalline ZnO:Co aggregates mostly perpendicular to the surface of the Si-substrate (Fig. S5). Dark field (DF) TEM images hinted at a columnar growth of ZnO:Co. High resolution TEM (HR-TEM) images of the sputtered ZnO:Co film on Si illustrate the existence of extensive dislocations and other growth defects. Different lattice distances of the hexagonal wurtzite-type ZnO structure ($P6_3mc$) could be identified (d= 0.247nm ($10\bar{1}1$), d= 0.263nm (0002), d= 0.282nm ($10\bar{1}0$)). The calculated lattice distance of 0.263 nm corresponds to the distance of the (0002) plane, thus indicating a preferred c-axis orientation of the layer. A conclusion on the relative orientation of the basal planes of the columns to each other is not possible. From the position of the reflexes in the selected area electron diffraction (SAED) pattern, an orientation of ZnO:Co columns to Si-substrate with $[002]_{Si\text{-}layer} \parallel [0002]_{ZnO:Co\text{-}substrate}$ can be deduced. TEM-EDX confirmed the elemental composition determined with SEM EDX and ICP-OES (Fig. S6)

The sputtered ZnO:Co films sputtered on FTO substrates were contacted in a custom made electrochemical cell (glassy carbon (GC) counter electrode, Ag|AgCl reference electrode, 1N KOH electrolyte) and used as working electrodes in cyclovoltametry (CV) experiments (Fig. 1a). Upon applying a potential, the ZnO:Co film changed its colour form green to brown and increasing catalytic currents were observed from cycle to cycle. The overpotential (η) to facilitate a current density (j) of 10 $mAcm^{-2}$ was determined to be 451.3 mV vs RHE in this setup.

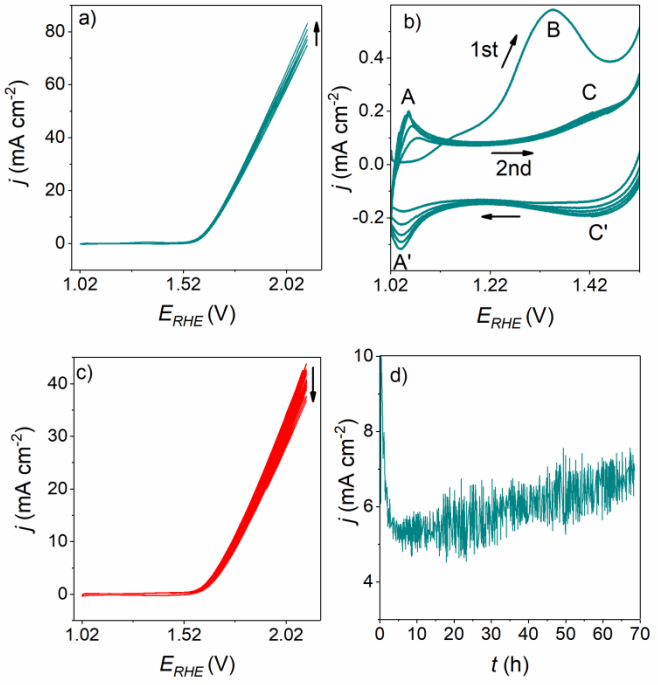

Figure. 1 a) Cyclovoltametry of ZnO:Co sputtered film onto FTO substrates. b) Enlarged oxidation and reduction waves of the sputtered ZnO:Co film c) CV of a ZnO:Co EPD film of comparable mass d) Chronoamperometric experiment of sputtered ZnO:Co film at η = 400 mV.

The catalyst film showed two characteristic reversible oxidation waves at lower potentials, which were attributed to the oxidation of $Co(OH)_2$ to CoOOH (A= 1.06 V_{ox} A' 1.04 V_{red}) and the further oxidation to Co(IV) species (C= 1.44 V_{ox} C'= 1.42 V_{red}; see Fig. 1b).[20,21] The initial scan did not feature these characteristic oxidation and reduction waves but showed a prominent irreversible oxidation wave at 1.35 V (B). The observed activation and activity were in good agreement with the observations made on particulate films of ZnO:Co.[19] When testing a ZnO:Co film grafted onto FTO by electrophoretic deposition (EPD) under comparable conditions, we observed pronounced oxidation waves as well, but much lower current densities were attained at the vertex potential and η= 10 mA cm^{-2} was significantly higher for this working electrode. To examine the stability of the *in-situ* formed WOC, an extended chronoamperometric experiment was performed with an sputtered ZnO:Co film (thickness ≈ 300 nm). The electrode was contacted in the custom made electrochemical cell and 1N KOH was electrolyzed for 72 hours. (Fig. 1d) Here the catalyst activation commences gradually over 6 h, with j further increasing from 6 to 9 $mAcm^{-2}$ over the course of 72 h.

Electron transparent cross sections were prepared after anodizing ZnO:Co films that had been sputtered on Si Wafers for

1h (Fig.2, see Fig. S7 for high resolution images). The electrocatalyst film after 1h exposure to electrolyte and voltage demonstrates the disorganization/dissolution of the upper part of the sputtered ZnO:Co film that has direct contact to the electrolyte solution during the chronoamperometric experiment. HR-TEM images reveal the formation of crystalline ZnO:Co nanoparticles with approx. 2 nm in size embedded in an amorphous matrix. Only a few large columnar crystallites from the electrocatalyst could be observed. Selected area electron diffraction (SAED) shows diffuse diffraction rings indicating that the ZnO:Co phase has a short-range-orientation and is only poorly crystalline. An exception, the relative intensity of (200) reflection (d= 0.213 nm) is remarkable strong. This observation was confirmed by performing a Fast Fourier Transformation (FFT) of the image data in regions 1 and 2. This is also supported by additional comparison with the EDX spectra of the sputtered layer before and after electrochemistry. Thereby, a strong enrichment of Co in contrast to a degradation of Zn could be observed.

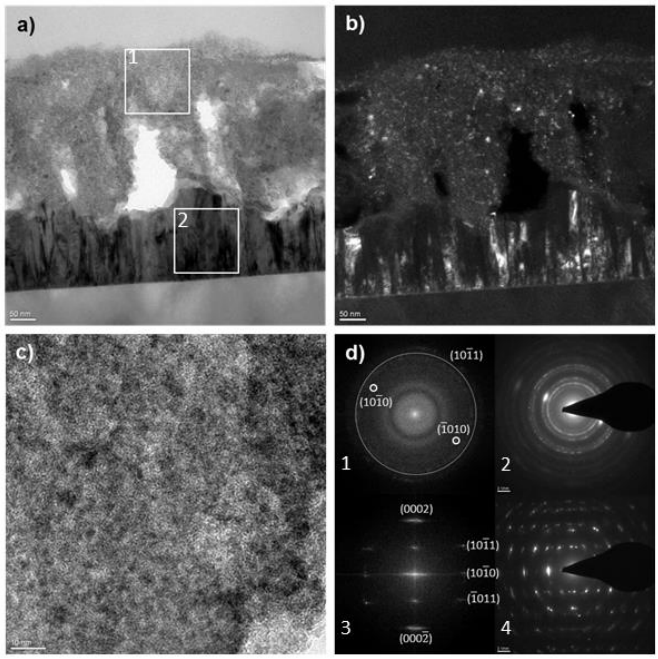

Figure 2. TEM analysis of a cross section from a partially anodized sputtered ZnO:Co film. a) TEM micrographs show a partial transformation to an amorphous material (1) form the polycrystalline electrocatalyst (2) b) DF-TEM shows monocrystalline components in the anodized and as prepared areas. c) HR-TEM micrographs of the amorphous region, d) FFT (1 & 3) and SAED (2 & 4) data from areas 1 and 2 seen in a).

As pointed out already, the formation of small crystalline Co enriched ZnO:Co particles in an amorphous matrix or an amorphous hull around these crystallites was also observed for the EPD-process after electrocatalysis.[16] In contrast, the lower part of the sputtered ZnO:Co remains unchanged in the columnar microstructure (and chemical composition). No changes were found at the interface of the sputtered layer to the Si substrate before and after electrochemistry. The sputtered ZnO:Co film shows a nearly complete dissolution after 10 hours of chronoamperometry (Fig. S8). As already shown in Fig. 2), the disaggregation of the original crystalline ZnO:Co columns and the formation of small particles with approx. 2 nm in size could be observed in the transformed layer partially consisting of nanoparticles. Thus, the mechanical instability of the sputtered ZnO:Co film increases. The dark-field pattern of the layer after electrochemistry imaged by the (10$\bar{1}$1) reflection of ZnO:Co clearly reveals that only a small amount of crystalline fragments are elongated and arranged parallel in direction perpendicular to the surface of the substrate layer surrounded by a strong amorphous matrix. On the basis of Fig. 2, we try to explain the change of the ZnO:Co columns during the electrochemistry experiments in the following. Small particles of 10 nm in size interspersed with holes of 2 nm in dimension and form a framework with columnar ZnO:Co aggregates that survived the electrochemical treatment. These particles could be regarded as a transitional state from the crystalline phase to the amorphous one. Only (10$\bar{1}$0), (10$\bar{1}$1) and (10$\bar{1}$2) reflexes could be measured. The *in- situ* formed amorphous phase is Zn depleted or, in other words, Co enriched, indicating the formation of new Co containing phases under OER conditions (Fig S5).

To gain further insight in the oxidation state of the amorphous portion of the in situ formed nanocomposite, the ZnO:Co sputtered films on FTO coated glass substrates were characterized *before* (as prepared) and *after* the electrochemical performance by near edge X-ray absorption fine structure (NEXAFS) spectroscopy at the Co K-edge as shown in Fig. 3.

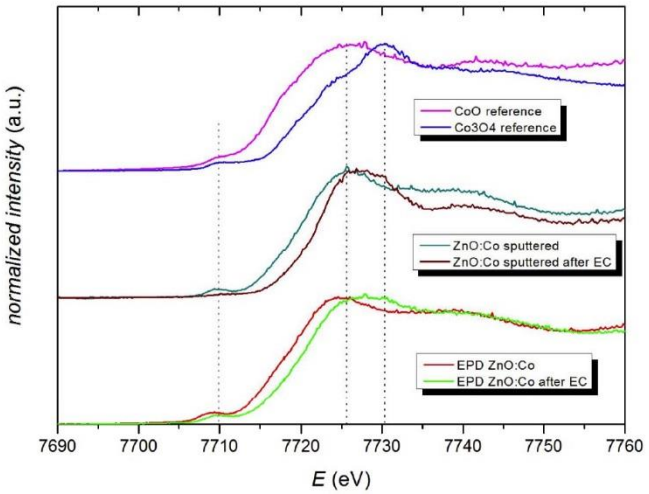

Figure 3 NEXAFS Co K-Edge data on sputtered ZnO:Co films (center) and ZnO:Co EPD films (bottom) as reference before and after electrochemical performance (EC). For comparison the NEXAFS spectra of CoO and Co_3O_4 are given as well.

The Co K-edge NEXAFS data shown in Fig. 3 are due to transitions of Co1s electrons into unoccupied Co4p states, Co1s→ Co4p. Hence, NEXAFS is sensitive to the oxidation state of the Cobalt because of a change in the partial density of unoccupied conduction band states (UDOS) and, additionally, due to a shift in the Co1s binding energy comparable to X-ray excited photoemission (XPS).[22] A change in the binding energy can be clearly seen in Fig.3, where the spectral shapes before and after the electrochemical performance are compared. The spectra of sputtered ZnO:Co films and ZnO:Co EPD films *before*

electrochemical performance were identical to that given in the report of Ney et al.[22] The distinct pre-edge feature at 7710 eV is associated with transitions between the 1s and bound p-hybridized d-states and is characteristic of Co^{2+} in tetrahedral coordination.[22] After the electrochemical performance, a shift of the absorption edge of about 4 eV to higher photon energy is observed revealing a change in oxidation state of the cobalt. The reference materials CoO [Co^{2+}] and Co_3O_4 [$Co^{2.7+}$; Co^{2+} and Co^{3+}] were also analysed in the same set-up and confirm a shift to higher energy in the presence of higher oxidized Co like Co^{3+}. A quantitative analysis of the respective concentrations remains difficult because of the coexistence of Co^{2+} and Co^{3+} oxidation states in the sample. However, it is clearly observed that the distinct pre-edge feature of pristine sputtered ZnO:Co film is almost lost during activation as compared to the pre-edge feature in the particulate EPD ZnO:Co film. This is suggesting a more quantitative phase transformation of the ZnO:Co crystallites in the sputtered films as compared to the crystallites in the EPD ZnO:Co film sample. Indeed, when comparing HR-TEM micrographs of the films after electrochemical performance (Fig S5), far less crystalline ZnO:Co is observed in the sputtered film sample. GI-XRD of the sputtered ZnO:Co films after electrochemical performance revealed a new reflex at 2θ = 19.8° (Fig. S7), which might indicate the formation of partially crystalline CoOOH, the Co^{3+} containing phase that is observed by NEXAFS on the electrochemical treated electrode. The Co^{2+} phases detected by NEXAFS after electrochemical performance are remnants of the ZnO:Co electrocatalyst, as well as $Co(OH)_2$ (see oxidation waves A, A' and C, C' in the CV, Fig.1). Apparently, the columnar crystallites with their large exposed facets are more susceptible to phase transformation induced by electrochemistry than the plate like ZnO:Co particles in the EPD film. This leads to a larger fraction of CoOOH on the electrochemical treated electrode, thus a more effective water oxidation system. Due to these morphological (columnar crystallites) and chemical (metastable ZnO:Co) properties of the sputtered electrocatalyst film, this material system is one of very few examples with a higher efficiency than a particulate electrocatalyst film with a high specific surface area.[16] The structural characterization of the sputtered ZnO:Co electrocatalyst films showed the transition at the surface and in the near-surface region of the polycrystalline ZnO:Co electrocatalyst material into a partially amorphous nanocomposite (ZnO:Co/$Co(OH)_2$/CoOOH). This transformation can be explained with the *Pourbaix*-diagrams for ZnO and CoO[23], wherein under the given pH and potential only Co^{II} forms insoluble $Co(OH)_2$ and CoOOH, whereas ZnO is dissolved. In previous studies on particulate films it was shown that Zn Ions leave the electrocatalyst, whereas insoluble $Co(OH)_2$ remains on the electrode surface and is oxidized to electrocatalytically active CoOOH. Once formed, the composite material is resistant towards the alkaline electrolyte and the anodization does not commence. This effect set in earlier in the sputtered film, preventing a complete transformation of the electrocatalyst in an electrocatalytically active phase. The columnar crystallites of ZnO:Co in the sputtered film were far more readily dissolved along the elongated c-axis, facilitating a more efficient transition into mostly amorphous $Co(OH)_2$/CoOOH. This high reactivity of the electrocatalyst material compensates effectively the low specific surface area of sputtered electrocatalyst thin films.

In this study, sputtered ZnO:Co thin films were morphologically examined as water oxidation catalyst before and after an electrochemical treatment. Sputtered ZnO:Co electrocatalyst films show the transition at the surface and in the near-surface region of the polycrystalline ZnO:Co film into a partially amorphous nanocomposite (ZnO:Co/$Co(OH)_2$/CoOOH). The columnar crystallites in the sputtered film with their large exposed facets are susceptible to electrochemically induced phase transformation. This leads to a larger amount of CoOOH on the electrochemically treated electrode surface, resulting in an effective water oxidation system. As a result of these morphological and chemical properties of the sputtered electrocatalyst film, this material system is one of the few examples with a higher efficiency than a particulate electrocatalyst film with a high specific surface area.

Notes and references

1 N. S. Lewis and D. G. Nocera, *Proc. Natl. Acad. Sci. U.S.A.*, 2006, **103**, 15729–15735.

2 see for example: M.B. Tahir, K.N. Riaz, A.M. Asiri, *Inter. J. Energy Res.*, 2019, **43** (11), 5747-5758; M.B. Tahir, M. Sagir, N. Abas *Inter. J. Hydrogen Energy,* **44**, 2019, 24690-24697.

3 H. Dau, C. Limberg, T. Reier, M. Risch, S. Roggan and P. Strasser, *ChemCatChem*, 2010, **2**, 724–761.

4 McCrory, Charles C L, S. Jung, I. M. Ferrer, S. Chatman, J. C. Peters and T. F. Jaramillo, *J. Am. Chem. Soc.*, 2015, **13**, 4347–4357.

5 S. Gholamrezaei, M. Ghanbari, O. Amiri, M. Salavati-Niasar, L. Kok Foong, *Ultrasonics Sonochemistry*, 2020 **61**, 104829.

6 Y. Zhang, B. Cui, C. Zhao, H. Lin and J. Li, *Phys. Chem. Chem. Phys.*, **15**, 7363–7369.

7 M. Fekete, R. K. Hocking, Chang, Shery L. Y., C. Italiano, A. F. Patti, F. Arena and L. Spiccia, *Energy Environ. Sci.*, 2013, **6**, 2222–2232.

8 a) M. W. Kanan and D. G. Nocera, *Science*, 2008, **321**, 1072–1075; b) A. Singh, Chang, Shery L. Y., R. K. Hocking, U. Bach and L. Spiccia, *Energy Environ. Sci.*, 2013, **6**, 579–586;

9 A. Goktas, F. Aslan, I.H. Mutlu, *Journal of Alloys and Compounds*, 2014, **615,** 5 765-778.

10 R. Sinha, R. Lavrijsen, M.A. Verheijen, E. Zoethout, H. Genuit, M.C.M. van de Sanden, A. Bieberle-Hütter, *ASC Omega,* 2019, **4** 9262-9270.

11 L. Jia, K. Harbauer, P. Bogdanoff, I. Herrmann-Geppert, A. Ramírez, R. van de Krol and S. Fiechter, *J. Mater. Chem. A*, 2014, **2**, 20196–20202.

12 K. Sun, Y. Kuang, E. Verlage, B. S. Brunschwig, C. W. Tu and N. S. Lewis, *Adv. Energy Mater.*, 2015, **5**, 1402276.

13 a) K. Sun, X. Pang, S. Shen, X. Qian, J. S. Cheung and D. Wang, *Nano letters*, 2013, **13**, 2064–2072; b) E. R. Young, D. G. Nocera and V. Bulović, *Energy Environ. Sci.*, 2010, **3**, 1726; c) Y. Zhan, M. Lu, S. Yang, C. Xu, Z. Liu and J. Y. Lee, *ChemCatChem*, 2016, **8**, 372–379; d) C. E. Frey, F. Kwok, D. Gonzáles-Flores, J. Ohms, K. A. Cooley, H. Dau, I. Zaharieva, T. N. Walter, H. Simchi, S. E. Mohney and P. Kurz, *Sustainable Energy Fuels,* http://pubs.rsc.org/en/content/articlepdf/2017/se/c7se00172j

14 T. M. Milão, J. F. A. Oliveira, V. D. Araújo and M. I. B. Bernardi, *J Therm Anal Calorim*, 2011, **103**, 873–877.

15 K. Ueda, H. Tabata and T. Kawai, *Appl. Phys. Lett.*, 2001, **79**, 988–990.

16 J. Pfrommer, M. Lublow, A. Azarpira, C. Göbel, M. Lücke, A. Steigert, M. Pogrzeba, P. W. Menezes, A. Fischer, T. Schedel-Niedrig and M. Driess, *Angew. Chem. Int. Ed.*, 2014, **126**, 5283–5287.

17 A. Azarpira, J. Pfrommer, K. Olech, C. Höhn, M. Driess, B. Stannowski, T. Schedel-Niedrig and M. Lublow, *J. Mater. Chem. A*, 2016, **4**, 3082–3090.

18 R. Klenk, A. Steigert, T. Rissom, D. Greiner, C. A. Kaufmann, T. Unold and M. C. Lux-Steiner, *Prog. Photovolt: Res. Appl.*, 2014, **22**, 161–165.

19 D. M. Jang, I. H. Kwak, E. L. Kwon, C. S. Jung, H. S. Im, K. Park and J. Park, *J. Phys. Chem. C*, 2015, **119**, 1921–1927.

20 I. G. Casella and M. R. Guascito, *J. Electroanal. Chem.*, 1999, **476**, 54–63.

21 J. G. McAlpin, Y. Surendranath, M. Dinca, T. A. Stich, S. A. Stoian, W. H. Casey, D. G. Nocera and R. D. Britt, *J. Am. Chem. Soc.*, 2010, **132**, 6882–6883.

22 A. Ney and M Opel and T C Kaspar and V Ney and S Ye and K Ollefs and T Kammermeier and S Bauer and K-W Nielsen and S T B Goennenwein and M H Engelhard and S Zhou and K Potzger and J Simon and W Mader and S M Heald and J C Cezar and F Wilhelm and A Rogalev and R Gross and S A Chambers, *New J. Phys.*, 2011, **13**, 103001.

23 a) J. Chivot, L. Mendoza, C. Mansour, T. Pauporté and M. Cassir, *Corr. Sci.*, 2008, **50**, 62–69; b) M. Pourbaix, *Atlas of electrochemical equilibria in aqueous solutions*, National Association of Corrosion Engineers, 1974;